Pergamon

Int. J. Mach. Tools Manufact. Vol. 36, No. 2, pp. 155–171, 1996

0890–6955/96$9.50 + .00

ON THE DESIGN OF EJECTORS FOR DEEP HOLE MACHINING

V. P. ASTAKHOV,† P. S. SUBRAMANYA† and M. O. M. OSMAN†

(*Received* 13 *April* 1994; *in final form* 20 *March* 1995)

Abstract—A comprehensive study of ejectors used in deep-hole drills was conducted in order to understand the role of the ejectors with annular nozzles in the tool design. An analytical method was used to derive the equation for the operating energy characteristic of ejectors. The experimental investigations were carried out to explain the ejector's optimal design parameters necessary to achieve maximum hydraulic efficiency. The experiments also defined the principal criteria and compared different types of ejector nozzles suitable for deep-hole drills. Further investigation revealed the precise location of the ejector nozzle(s) in the deep-hole drill assembly and helped clarify the capabilities of the ejectors.

NOMENCLATURE

A_h	total cross-sectional area of the outlet holes of the drill head
A_{in}	cross-sectional area of the inner tube
A_n	cross-sectional area of the nozzle (Table 1)
A_1	cross-sectional area of the ejector nozzle
A_2	cross-sectional area of the mixing chamber
D_b	internal diameter of the boring bar
d_{b1}, d_{b2}	diameters of the inner tube in Fig. 12
d_{e1}, d_{e2}	equivalent diameters of the annular channels restricted by diameters D_b, d_{b1}; and D_b and d_{b2}, respectively
d_{it}	diameter of the inner tube in Fig. 16
d_{mc}	diameter of the mixing chamber
Eu	Euler number
f_{ag}	friction factor for the annular channel
g	gravity constant
H_{AB}, H_{BC}, H_{BD}	hydraulic heads at parts AB, BC and BD, respectively
H_{vac}	vacuum pressure in the mixing chamber
H_Σ, $H_{\Sigma BCD}$	total hydraulic heads at the inlet (Point A, Fig. 12) and at point B
H_1	operating hydraulic head
H_2	hydraulic head past ejector
h	relative head
L	length of the annular channel in Fig. 12
l_d, l_{mc}	length of the diffuser and mixing chamber, respectively
l_e, l_o	length of the parts of the annular channel in Fig. 12
m	modulus of the geometrical similarity
n	number of the ejector nozzles (Table 1)
P_a, P_b, P_c	pressures at the sections a–a, b–b, c–c (Fig. 2), respectively
Q_Σ	necessary total flow rate
$Q_{\Sigma BCD}$	total flow rate for parts BC and BD (Fig. 12)
Q_0	re-circulation flow rate
Q_1	operating flow rate
Q_2	swarf flow rate past ejector
q	relative flow rate
S_{AB}, S_{BC}, S_{BD}	hydraulic resistance coefficients for part AB, BC and BD, respectively
Z_A, Z_B, Z_C	elevations of points A, B and C, respectively
v_{cr}	critical velocity of the cutting fluid
v_N	velocity of the cutting fluid at the ejector nozzle
v_1, v_2	velocities of the cutting fluid at the sections 1–1 and 2–2, respectively (Fig. 2)
α	angle of the conical part of the ejector nozzle
α_a, α_b, α_c	velocity coefficients in the sections a–a, b–b and c–c (Fig. 2), respectively
α_d	diffuser angle
α_N	velocity coefficient in the ejector nozzle
β	wing angle of the ejector nozzle

†Department of Mechanical Engineering, Concordia University, Montreal, Quebec, Canada H3G 1M8.

Δh	head loss of the cutting fluid-chips mixture along the distance between the machining zone and the ejector nozzle
Δp	pressure drop in the ejector nozzle
δ_0	nozzle width along the drill axis (Fig. 16)
δ_1, δ_2	thickness of the inner tubes with diameter d_{b1} and d_{b2}, respectively (Fig. 12)
ζ_c	pressure loss coefficient of the connector
ζ_{oh}	pressure loss coefficient of the outlet holes of the drill head
ζ_N, ζ_{in}, ζ_{mc}, ζ_d	pressure loss coefficients of the ejector nozzle, of the inlet, of the mixing chamber and of the diffuser, respectively
ζ_Σ	total pressure loss coefficient of the re-circulation flow rate
η_E	hydraulic efficiency of the ejector
μ	discharge coefficient of the ejector nozzle
ρ_c	mass density of the cutting fluid
Σh	total hydraulic head loss past the ejector

1. INTRODUCTION

The machining of holes of high length-to-diameter ratio to high standards of size, parallelism, straightness and surface finish has always presented problems. One of the most significant technological advances made during the past 40 years to help solve these problems has been the development of the BTA (the Boring and Trepaning Association) Technique. Figure 1(a) shows the principle of the BTA deep-hole drilling process. The BTA tool consists of a boring bar, a single or multi-edged drill head and a pressure head. During drilling, the cutting fluid is fed through the inlet in the pressure head and flows through the annular channel, between the boring bar and the bore wall to the drill head. After performing its cooling and lubricating actions in the machining zone, the cutting fluid detects chips through the interior of the drill head and out through the boring bar. The returning chips do not have contact with the bore wall and an excellent bore finish is obtained under optimal drilling conditions. Even though a significant amount of research has been done in this field, a lot more research is required to establish a methodology for the efficient designing of deep-hole drilling tools. One of the main problems associated with deep-hole drilling is chip removal from the machining zone. To overcome this problem the machining zone is flooded with the cutting fluid under high pressure. However, this does not always solve the problem of high energy losses that take place in the hydraulic systems of these drills, which result in a significant drop in the cutting fluid pressure. Another problem is that this process can be used only on specific deep-hole machines, not common machine tools. The Coromant Ejector drilling tools were introduced to overcome these problems in developing a deep-hole drilling technique. Figure 1(b) shows the principle of the Ejector drilling process. The cutting fluid that is necessary for transporting the chips, as well as for cooling and lubricating the cutting edge and supporting pads, is passed to the drill head by means of a two-tube system. The outer tube (boring bar) takes up the torque and the feed force. The inner tube has an annular ejector nozzle through

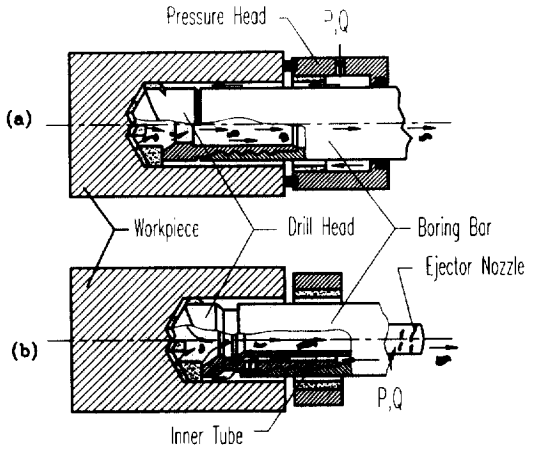

Fig. 1. BTA (a) and ejector (b) deep-hole drilling.

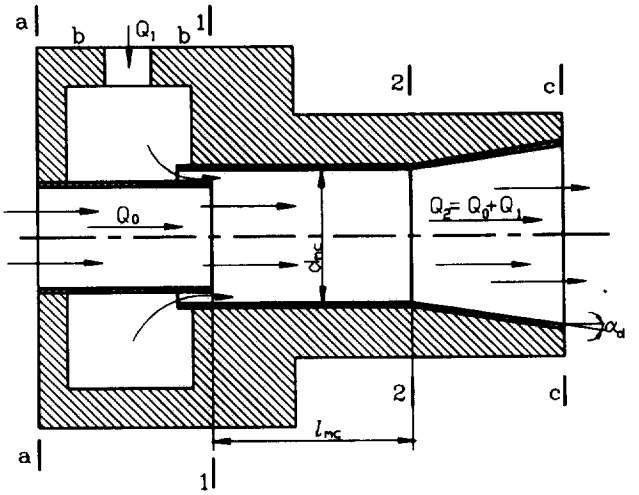

Fig. 2. Schematic diagram of the ejector with the annular nozzle.

which a portion of the cutting fluid is passed, creating a partial vacuum (the ejector effect). The remaining cutting fluid flows through an annular channel, between the boring bar and the inner tube over the drill head and is diverted back through the bore of the inner tube, where it is sucked back along with the chips. In this way, the circuit of the cutting fluid is simplified and the need for a complicated sealing unit overcome.

It is no longer necessary to create a seal between the workpiece and the starting bush, the starting bush can be up to 1 mm away from the face of the workpiece, therefore, Ejector drills can be used on most standard machine tools. The performance of an Ejector drill depends, to a large extent, upon the efficiency of its ejector, which defines the energy distribution in the drill's hydraulic system [1–3].

This paper presents the results of theoretical and experimental investigations of the deep-hole drill's ejectors with annular nozzles.

2. BASIC ENERGY PARAMETERS

The schematic diagram of the ejector with the annular nozzle is shown in Fig. 2. The operating regime of this ejector is characterized by the following parameters:

(a) *Dimensional parameters.* The most relevant dimensional parameters are: recirculation flow rate, Q_0; operating flow rate, Q_1; operating hydraulic head, H_1; swarf flow rate past ejector, Q_2; $= Q_0 + Q_1$; swarf head past ejector, H_2; cross-sectional area of the ejector nozzle, A_1; cross-sectional area of the mixing chamber, A_2.

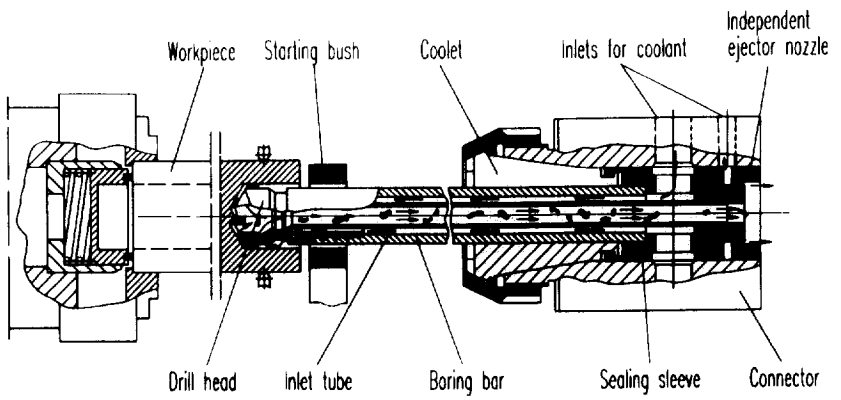

Fig. 3. Ejector drill with the "independent" ejector.

(b) *Non-dimensional parameters.*
(i) relative head

$$h = H_2/H_2 \tag{1}$$

(ii) relative flow rate

$$q = Q_0/Q_1 \tag{2}$$

(iii) modulus of the geometrical similarity

$$m = A_2/A_1 \tag{3}$$

(iv) hydraulic efficiency

$$\eta_E = q\frac{h}{1-h}. \tag{4}$$

3. OPERATING ENERGY CHARACTERISTIC OF THE EJECTOR

The operating energy characteristic of the ejector can be derived by using two different approaches: (a) the energy analysis and (b) the impulse theorem [4]. Using the energy analysis seems to be reasonable, as it avoids those problems connected with separating the influence of each ejector's design parameters on its energy characteristic [5].

Basic energy relations can be obtained by analyzing the flows of cutting fluid in sections a–a, b–b, c–c (Fig. 2):

$$H_2 + \left(\frac{p_c}{\rho_c g} + \frac{\alpha_c v_a^2}{2g}\right) - \left(\frac{p_a}{\rho_c g} + \frac{\alpha_a v_a^2}{2g}\right) \tag{5}$$

$$H_1 + \left(\frac{p_b}{\rho_c g} + \frac{\alpha_b v_b^2}{2g}\right) - \left(\frac{p_a}{\rho_c g} + \frac{\alpha_a v_a^2}{2g}\right). \tag{6}$$

Then, the relative head is:

$$h = \frac{H_2}{H_1} = \frac{\left(\frac{p_c}{\rho_c g} + \frac{\alpha_c v_c^2}{2g}\right) - \left(\frac{p_a}{\rho_c g} + \frac{\alpha_a v_a^2}{2g}\right)}{\left(\frac{p_b}{\rho_c g} + \frac{\alpha_b v_b^2}{2g}\right) - \left(\frac{p_a}{\rho_c g} + \frac{\alpha_a v_a^2}{2g}\right)}. \tag{7}$$

Here, α_a, α_b and α_c are velocity coefficients in sections a–a, b–b and c–c (Fig. 2), respectively. The parameters of the flows in sections a–a, b–b and c–c can be expressed through the parameters of the flow in the beginning of the mixing chamber (section 1–1, Fig. 2), as follows:

$$\frac{p_b}{\rho_c g} + \frac{\alpha_b v_b^2}{2g} = \frac{p_1}{\rho_c g} + \frac{\zeta_N v_N^2}{2g} \tag{8}$$

$$\frac{p_a}{\rho_c g} + \frac{\alpha_a v_a^2}{2g} = \frac{p_1}{\rho_c g} + \frac{\alpha_N v_N^2}{2g} + \frac{\zeta_{in} v_N^2}{2g} \tag{9}$$

$$\frac{p_c}{\rho_c g} + \frac{\alpha_c v_c^2}{2g} = \frac{p_1}{\rho_c g} + \frac{\alpha_1 v_1^2}{2g} - (\zeta_{mc} + \zeta_d)\frac{v_2^2}{2g}. \tag{10}$$

Substituting equations (8)–(10) to equation (7), considering that the fluid velocity at the ejector nozzle, v_N, is much higher than the velocity at section 1–1, v_1 and, finally, assuming that the kinetic energy of the cutting fluid flow in the section 1–1 is approximately equal to the kinetic energy of the operating cutting fluid flow [1], we arrive at:

$$h = \frac{m^2 - (\zeta_{mc} + \zeta_d)(1+q)^2 - q^2(1+m)^2(1+\zeta_{in})}{(1+\zeta_N)m^2 - q^2(1+m)^2(1+\zeta_{in})}. \tag{11}$$

This equation represents the operating energy characteristic of the ejector when the energy parameters of the re-circulation and operating flows are independent. This case corresponds to the ejector drill with the "independent" ejector as shown in Fig. 3 [6]. Here, the cutting fluid necessary for the transportation of chips and the cooling and lubricating of the cutting edge and supporting pads is fed to the machining zone through the pressure head and the annular channel between the boring bar and the inner tube. The other cutting fluid flow (from the other pump) is fed to the barb fitting, passes through the ejector nozzle and creates a partial vacuum in the mixing chamber. This causes the cutting fluid from the machining zone to be sucked back along with the chips. As our experience shows, this design is preferable because it saves energy and provides the possibility to regulate the operating regime in the wide limits, depending on the particular tool geometry and workpiece material. Nevertheless, the current market still only offers those ejector drills using the "dependent" ejector design [Fig. 1(b)]. In such drills, the energy parameters of the re-circulation and operating flow rates are dependent. If we express the flow parameters in the different sections through the flow parameters at the beginning of the mixing chamber (section 1–1, Fig. 2), we have:

$$\frac{p_a}{\rho_c g} + \frac{\alpha_a v_a^2}{2g} = \frac{p_1}{\rho_c g} + \frac{\alpha_a v_N^2}{2g} - \zeta_\Sigma \frac{v_N^2}{2g} \tag{12}$$

$$\frac{p_b}{\rho g} + \frac{\alpha_b v_b^2}{2g} = \frac{p_1}{\rho g} + \frac{\alpha_N v_N^2}{2g} - \zeta_\Sigma \frac{v_N^2}{2g} \tag{13}$$

$$\frac{p_c}{\rho_c g} + \frac{\alpha_c v_c^2}{2g} = \frac{p_1}{\rho_c g} + \frac{\alpha_1 v_1^2}{2g} - (\zeta_{mc} + \zeta_\Sigma)\frac{v_2^2}{2g}. \tag{14}$$

Here ζ_Σ is the total pressure loss coefficient of the re-circulation flow rate [7].

Expressing velocities v_N, v_2 and v_0, in equations (12)–(14) through the corresponding flow rates and assuming that $\alpha_N = \alpha_a = \alpha_1 = 1$, we obtain:

$$h = \frac{m^2 - (\zeta_{mc} + \zeta_d)(1+q)^2 - q^2(1+m)^2(1+\zeta_{in})}{(1+\zeta_N)m^2 - q^2(1+m)^2(1+\zeta_{in})}. \tag{15}$$

Equations (11) and (15) are the main equations for calculating the ejector's energy characteristics during operation. Our experimental investigations show that the value of $\zeta_{in} = 0.10$–0.12 can be accepted in calculations.

4. SELECTION OF EJECTOR NOZZLE TYPE

Through the analysis of the different types of ejector nozzles (see Appendix A), we recommend the combined ejector nozzle which contains both the conical and cylindrical parts. The ejector drill with this nozzle is shown in Fig. 4, where the selected angle of the conical part (α) is equal to 10–15°, based on the following:

(1) If $\alpha > 10°$, it leads to an increase in the axial size of the entire ejector and the connection between the tubular parts of the inner tube is weakened.

(2) If $\alpha > 15°$, it leads to increased energy loss in the nozzle and the mixing chamber

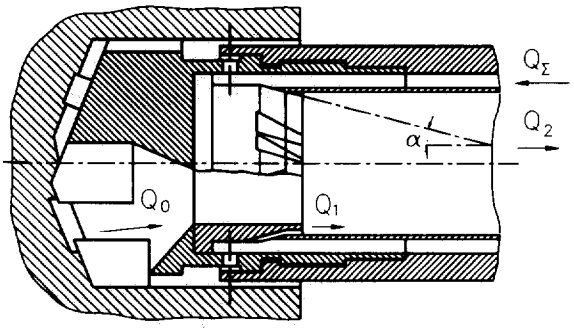

Fig. 4. Ejector drill with the combined ejector nozzle.

because the operating flow mixes with the re-circulation flow without the preliminary adjustment of their velocities.

In order to understand the chips' behavior while the re-circulation and operating flows are mixing, the flow structures in the mixing chamber are investigated. The experiments were conducted on different types of ejector nozzles and the best results occur with combined and vortex-combined ejector nozzles. The flow structures of the nozzles in the mixing chamber are shown in Figs 5(a)–(c). Here, it can be seen that the presence of chips in the cutting fluid (in the re-circulation flow) has a significant effect on the flow structure in the mixing chamber. While the chips are present, there

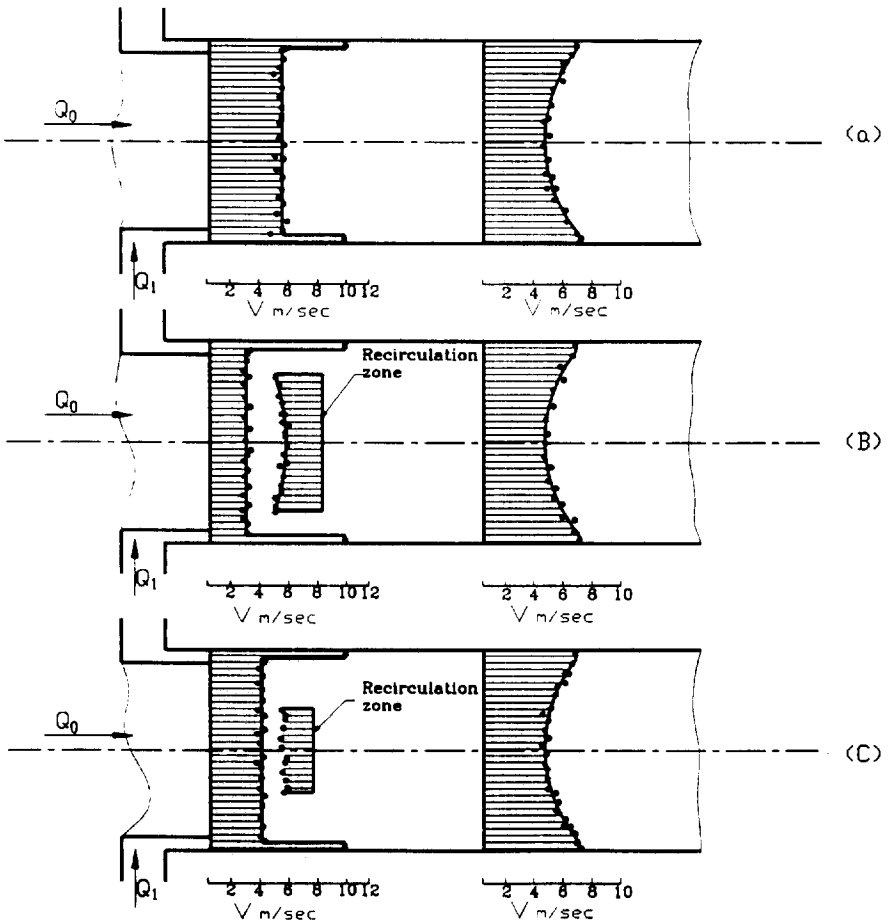

Fig. 5. Flow structure in the mixing chamber: Q_1 = 70 l/min, d_{mc} = 36 mm, m = 8. (a) Combined ejector nozzle with pure re-circulation cutting fluid; (b) combined ejector nozzle with cutting fluid–chip mixture; (c) vortex combined ejector nozzle with cutting fluid–chip mixture.

appears a re-circulation zone in the mixing chamber. The flow in this zone is in the opposite direction to the re-circulation and operating flows, and contact between the chips from the machining zone and the re-circulation zone takes place. Usually when machining medium carbon steel, the chips do not contract and the re-circulation zone does not affect the drilling process. On the other hand, machining aerospace materials (stainless steels, low carbon alloys, etc.) results in chip contraction, causing the influence of the re-circulation zone to halt the drilling process altogether. This will also usually cause drill head damage if the drilling machine does not have the safety system equipped with a transducer for the chips in the chip removal channels. Therefore, while drilling aerospace materials, it is reasonable to use the vortex-combined ejector nozzle. The ejector drill with this nozzle is shown in Fig. 6. Here, angle α of the conical part of the nozzle, along with the combined nozzle and wing-angle β, is selected as equal to 20–30°. This choice is based on the following considerations:

(1) If $\beta < 20°$, then the recalculation zone is growing, reducing the effectiveness of the nozzle.

(2) If $\beta > 30°$, then the tangential component of the operating flow velocity is growing, leading to increased energy loss during the mixing of the re-circulation and operating flows.

5. THE LENGTH AND DIAMETER OF THE MIXING CHAMBER

The length of the mixing chamber, l_{mc} (Fig. 2), is one of the main design parameters of the ejector [1]. Experiments were conducted to establish optimum conditions with minimum energy loss in the mixing chamber. These experiments used the special sectional mixing chamber set-up [1]. During the initial stages, the unique energy characteristic, $h = f(q)$, became apparent and emphasized the ejector to be dependent of the hydraulic head of the operating flow (Fig. 7). In the second stage, the section-type mixing chamber was used and the experimental characteristics $h = f(q,m)$, under different ratio l_{mc}/d_{mc} are obtained [Figs 8(a)–(d)]. The optimal length of the mixing chamber was chosen, corresponding to the maximum relative head, h, under constant relative flow rate, q; that is, under maximum energy efficiency of the ejector under given modulus m. Using these points, the relationship $(l_{mc}/d_{mc})_{opt} = f(m)$ was obtained (Fig. 9).

6. EFFICIENCY OF EJECTORS WITH ANNULAR NOZZLES—GENERAL ENERGY CHARACTERISTICS

The efficiency of ejectors with annular nozzles, $\eta_E = f(q,m)$ is shown in Fig. 10. It is observed that maximum efficiency is achieved when $m = 3.5$–4.0. It should be noted that in commercial ejector drills, the modulus is usually >10. Based upon maximum efficiency, the general energy characteristic $h - f(q,m)$ is obtained (Fig. 11).

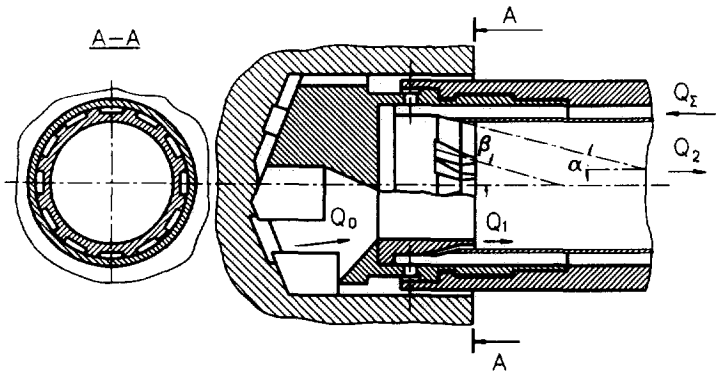

Fig. 6. Ejector drill with the vortex-combined ejector nozzle.

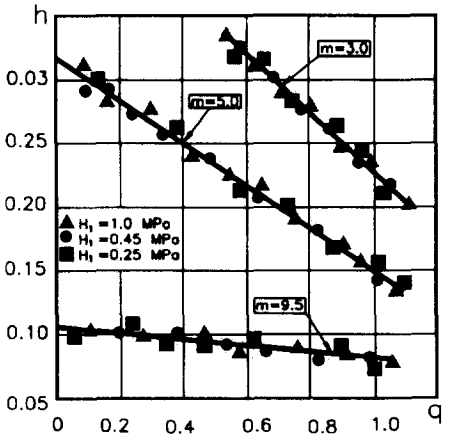

Fig. 7. Effect of the operating head, H_1, on the characteristic $h = f(q)$.

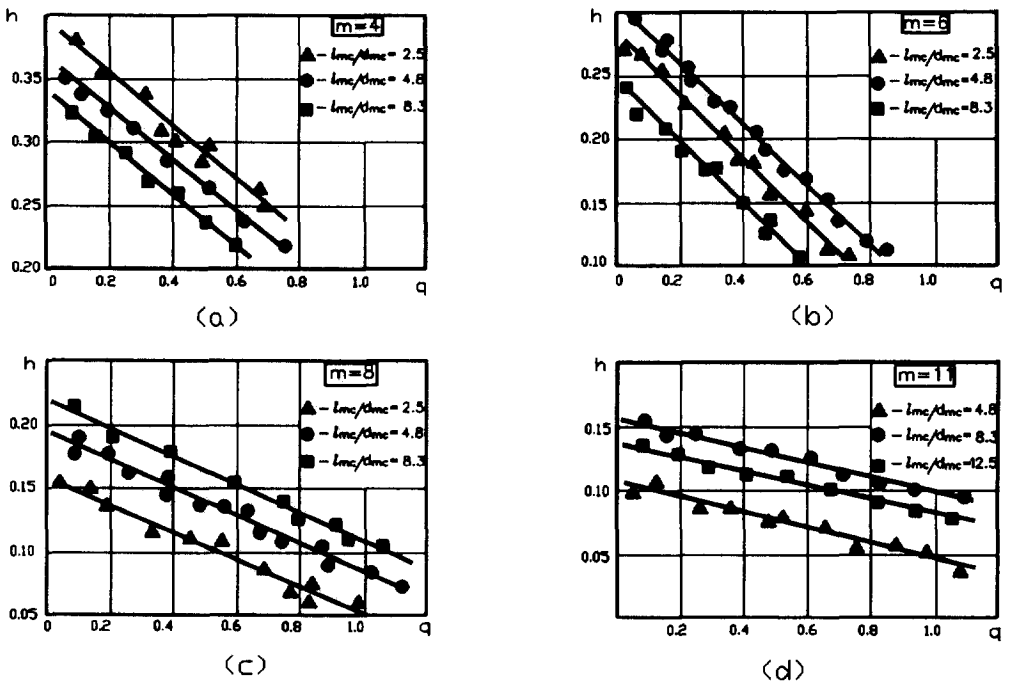

Fig. 8. Effect of ratio l_{mc}/d_{mc} on the characteristic $h = f(q)$.

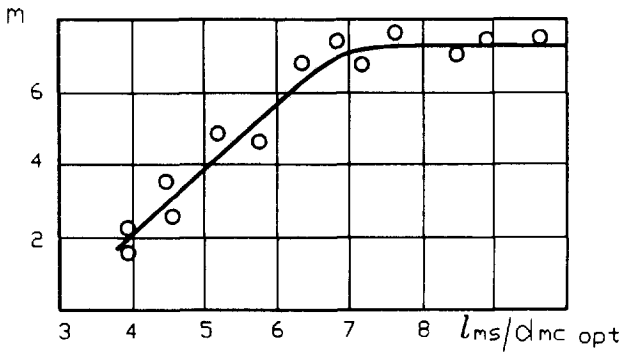

Fig. 9. Effect of the modulus m on the ratio $(l_{mc}/d_{mc})_{opt}$.

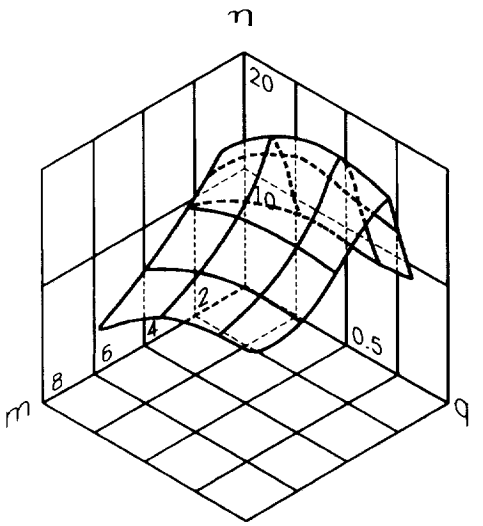

Fig. 10. Influence of the relative flow rate, q, and modulus m on the energy efficiency of the ejector.

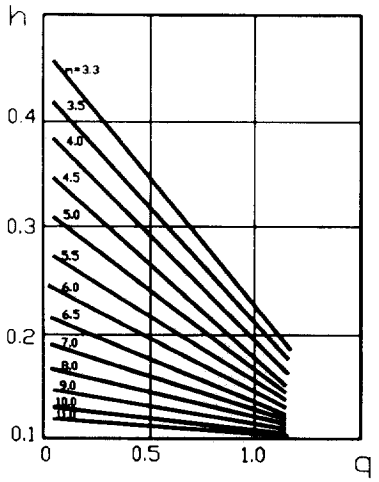

Fig. 11. General energy characteristics of ejectors with annular nozzles under maximum hydraulic efficiency.

7. POSITION OF EJECTORS IN THE HYDRAULIC SYSTEM OF DRILLS

Positioning of the ejector nozzle in the hydraulic system of drills plays a vital role in chip removal conditions. Currently, ejector drills are commercially available with two nozzle locations:

(1) The nozzle located in the drill head. In this case, the ejector has the minimal length of the re-circulation channel, therefore the maximal suction capability. Simultaneously, the operating pressure is not enough to reach optimal operating conditions because: (a) pressure is defined by the hydraulic resistance of the machining zone only and (b) there is significant pressure loss along the annular channel, between the connector and the drill head.

(2) The nozzle located in the connector. Here, the operating pressure can be high enough. However, this position of the ejector has its own disadvantages: (a) the length of the drill is restricted by the suction capability of the ejector nozzle and, as a rule, cannot exceed two meters and (b) the length of the mixing chamber is less than optimal, reducing the effectiveness of the ejector.

Hence, the positioning of the ejector along the inner tube has to be defined through specific hydraulic calculation.

The schematic diagram of the ejector drill is shown in Fig. 12. Inlet coolant annular clearance can be classified into three regions: (1) AB is the part from the inlet section (corresponding to Point A), to the ejector nozzle (Point B); (2) BD corresponds to the nozzle, and connects the annular channel ($D_b - d_{b2}$) to the chip removal channel and (3) BC runs from the ejector nozzle (Point B) to the exit section of the outlet holes of the drill head (Point C). The equations for the hydraulic heads of these regions are:

$$H_{AB} = (Z_B - Z_A) + S_{AB}Q^2 \tag{16}$$

$$H_{BC} = (Z_C - Z_B) + S_{BC}Q^2 \tag{17}$$

$$H_{BD} = S_{BD}Q^2\,, \tag{18}$$

where Z_A, Z_B and Z_C are the elevations of points A, B and C, respectively, from datum m; S_{AB}, S_{BC} and S_{BD} are the hydraulic-resistant coefficients of the above-mentioned parts (s/m^2).

The hydraulic resistance coefficient for Section AB is:

$$S_{AB} = \left(\zeta_c + f_{ag1}\frac{l_e}{d_{e1}}\right)\frac{1}{128\,(D_b^2 - d_{b1}^2)^2}\,, \tag{19}$$

where ζ_c is the pressure loss coefficient of the connector; f_{ag1} is the friction factor for the annular channel, restricted by diameters D_b and d_{b1}; l_e is the length of the annular channel from the inlet to Point B (m); d_{e1} is the equivalent diameter of the annular channel (m). This diameter can be calculated as follows:

$$d_{e1} = \sqrt{(D_b^2 - d_{b1}^2)}\,. \tag{20}$$

The hydraulic-resistant coefficient for Section BC is:

$$S_{BC} = f_{ag1}\frac{l_o}{d_{e2}}\frac{1}{128\,(D_b^2 - d_{b2}^2)^2} + \frac{\zeta_{oh}}{2gA_h^2} \tag{21}$$

where f_{ag1} is the friction factor for the annular clearance, restricted by diameters D_b and d_{b2}; l_o and d_{e2} are the length and equivalent diameter of this clearance (m); ζ_{oh}

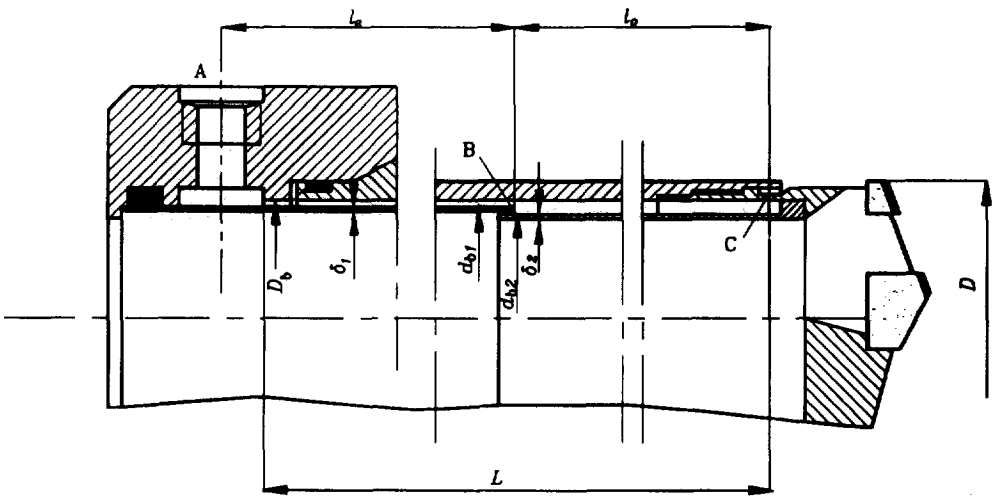

Fig. 12. Schematic diagram of the ejector drill.

is the pressure loss coefficient of the outlet holes of the drill head; A_h is the total cross-sectional area of these holes.

The hydraulic-resistant coefficient for Section BC is:

$$S_{BD} = \frac{1}{128\left[(d_{b1} - \delta_2)^2 - d_{b2}^2\right]^2 \mu}, \tag{22}$$

where δ_2 is the thickness of the inner tube (Fig. 12) and μ is the discharge coefficient of the ejector nozzle.

Sections BC and BD are connected in parallel. Equations (17) and (18) can be summarized by the coolant flow rate:

$$Q_{\Sigma_{BCD}} = \sqrt{\left[\frac{H_{BC} - (Z_c - Z_B)}{S_{BC}}\right]} + \sqrt{\left(\frac{H_{BD}}{S_{BD}}\right)} \tag{23}$$

and the hydraulic heads on these sections are $H_{BC} = H_{BD} = H_{\Sigma BCD}$. For horizontal drills $Z_c = Z_B$ and the flow rate is:

$$Q_{\Sigma_{BCD}}^2 = \frac{H_{\Sigma BCD}}{S_{BC}} + 2H_{\Sigma BCD}\sqrt{\left(\frac{1}{S_{BC}S_{BD}}\right)} + \frac{H_{\Sigma BCD}}{S_{BD}}. \tag{24}$$

It is obvious that the flow rate $Q_{\Sigma BCD}$ is equal to the inlet flow rate Q_Σ. Then:

$$H_{\Sigma_{BAD}} = \left(\frac{1}{\frac{1}{S_{BC}} + 2\sqrt{\left(\frac{1}{S_{BC}S_{BD}}\right)} + \frac{1}{S_{BD}}} + S_{AB}\right) Q_\Sigma^2. \tag{25}$$

Sections AB and Σ_{BCD} are connected in series. Allowing $Z_A = Z_B$ (horizontal drill location), equations (16) and (25) summarize the hydraulic heads as follows:

$$H_\Sigma = \left(\frac{1}{\frac{1}{S_{BC}} + 2\sqrt{\left(\frac{1}{S_{BC}S_{BD}}\right)} + \frac{1}{S_{BD}}} + S_{AB}\right) Q_\Sigma^2. \tag{26}$$

Equation (26) reveals the relationship between the inlet hydraulic head (H_Σ) and the flow rate (Q_Σ). Equation (25) defines the hydraulic head at the front end of the ejector nozzle.

The pressure loss coefficients ζ_c ζ_{oh}, and the friction factor f_{ag} are determined experimentally by using a special method [8] and a tailored experimental setup [9] (Figs 13–15).

The equations for the coefficients of hydraulic resistance for Sections AB and BC [equations (19) and (21)] are written for the most common location of the ejector nozzle, between the connector and the drill head. Using these equations, it is possible to define the position of the ejector in the hydraulic system of a drill and to calculate the inlet flow rate and pressure of the cutting fluid, as shown in Appendix B.

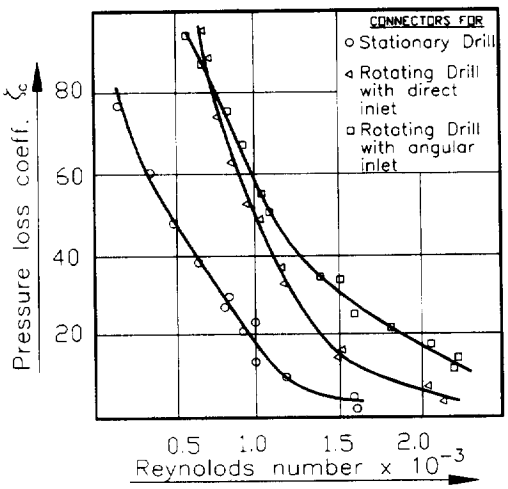

Fig. 13. Pressure loss coefficients ζ_c vs Reynolds numbers.

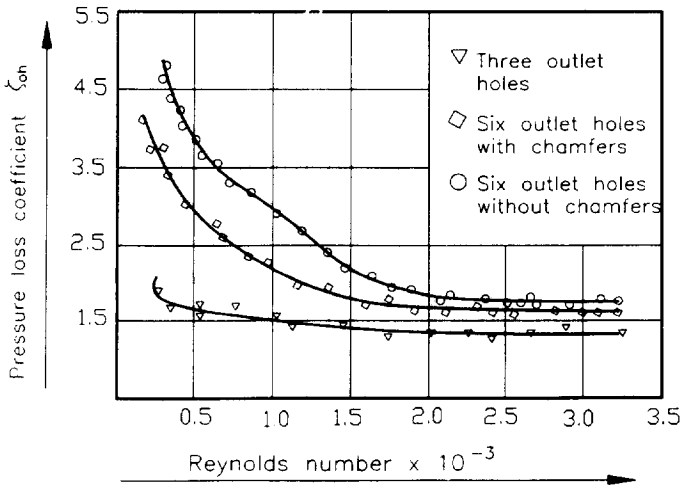

Fig. 14. Pressure loss coefficients ζ_{oh} vs Reynolds numbers.

8. CONCLUSIONS

Ejectors with annular nozzles can be used to improve the chip removal in deep-hole drills. A comprehensive analysis of ejectors used in deep-hole drills is provided to understand better the role and place of the ejector in tool design. Three non-dimensional characteristics define the operating regime of the ejector: relative head, relative flow rate, and modulus of the geometrical similarity. The energy principle is employed to derive equations for the operating energy characteristic for both independent and dependent ejectors. Analysis of the different types of ejector nozzles provides support to the recommendation for deep-hole drills, the combined (with the angle of the conical part equalling 12°) and vortex-combined (with the angle of the conical part equalling 12° and the wing angle equalling 20–30°) ejector nozzles. It was confirmed that the operating energy characteristic for ejectors with annular nozzles is independent from the operating head. The maximum hydraulic efficiency is achieved when the modulus of the geometrical similarity is selected within the range of 3.5–4.0 and the relative flow rate is selected between 0.4 and 0.6. Positioning of the ejector nozzle in the hydraulic system of the drills plays a vital role in the chip removal conditions and must be calculated using the proposed method.

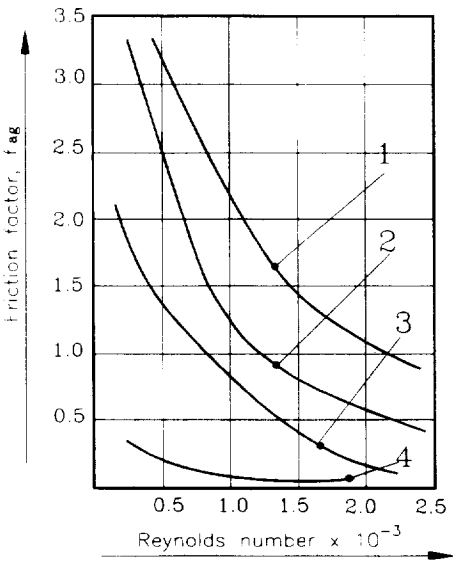

Fig. 15. Friction factors vs Reynolds numbers for the annular channels: (1) oil, $\nu_{50} = 0.17 \times 10^{-4}$ m²/sec; (2) oil-based coolant MR3, $\nu_{50} = 0.17 \times 10^{-4}$ m²/sec; (3) oil-based coolant Shell Haria H" and (4) water-based coolant.

Acknowledgements—The financial support of The Natural Science and Engineering Council of Canada as well as the support of El Formation de charters d'action concrete du Quebec are gratefully acknowledged.

REFERENCES

[1] V. P. Astakhov and A. M. Scorupco. Experiments into chip removal systems in deep-hole drilling (in Russian), *Metallorezushie Stanky* **10**, 58–62 (1982).
[2] V. P. Astakhov, Fundamental evaluations of machine-tool cooling systems for deep-hole drilling (in Russian), *Metallorezushie Stanky* **12**, 63–66 (1984).
[3] V. P. Astakhov, J. Frazao and M. O. M. Osman, On the design of deep-hole drills with non-traditional ejectors, *Int. J. Prod. Res.* **29** (11), 2297–2311 (1991).
[4] V. P. Astakhov, Modeling of thermo-hydraulic processes in technological systems of deep-hole machining (in Russian), *Metallorezushie Stanky* **18**, 70–74 (1990).
[5] A. P. Gnatuk, V. P. Astakhov and A. A. Chegodar, Experiments into energy parameters of coolant in hydraulic systems of deep-hole drills (in Russian). *Izvestia Vuzov. Mashinistroenie* No. 12, 113–118 (1989).
[6] G. M. Petrosjan, A. L. Airikjan and V. P. Astakhov, The ejector drill (in Russian), U.S.S.R. Patent No. 854608, GKNT, U.S.S.R. (1981).
[7] U. N. Suhorucov and V. P. Astakhov, Basic calculations of ejectors for deep-hole drills (in Russian), *Rezanie i Instrument* **29**, 23–26 (1983).
[8] V. P. Astakhov, A. L. Airikjan and A. M. Scorupco. Experimental method for investigation of hydraulic systems of ejector drills (in Russian), U.S.S.R. Patent No. 1041232, CGNT, U.S.S.R. (1983).
[9] V. P. Astakhov and A. L. Airikjan. Experimental setups for hydraulic systems of ejector drills (in Russian), U.S.S.R. Patent No. 1006091, GCNT, U.S.S.R. (1983).
[10] L. S. Egelson, Modeling (in Russian). *Soviet Sci.*, (1952).
[11] V. P. Astakhov and A. M. Scorupco, Basic calculations of special ejectors (in Russian), UkrNEENTE No. 2404-Yk, (1985).
[12] V. P. Astakhov, P. S. Subramanya and M. O. M. Osman, Theoretical and experimental investigations of coolant flow in inlet channels of the BTA and ejector drills, *Proc. Instn Mech. Ingr* **209**, pp. 211–220 (1995).
[13] V. P. Astakhov, P. S. Subramanya and M. O. M. Osman, An investigation of the cutting fluid flow in self-piloting drills, *Int. J. Mach. Tools Manufact.* **35**(4), 547–563 (1995).

APPENDIX A: INVESTIGATION OF THE DIFFERENT TYPES OF EJECTOR NOZZLES

Energy evaluations of the different types of design of ejector nozzles can be done using the relation $h = f(q)$. However, the design evaluation depends on the configuration and the length of the mixing chamber, whether there is a diffuser, etc. Consequently, it is difficult to separate the influence of the ejector nozzle itself. Because of this, a different method of evaluation is used.

The discharge coefficient of the ejector nozzle can be found using this recognized relation [10, 11]:

$$\mu = \frac{1}{\sqrt{(\alpha_N + \zeta_N)}} \tag{27}$$

Assuming uniform inlet nozzle flow ($\alpha_N = 1$), we have:

$$\mu = \frac{1}{\sqrt{(1 + \zeta_N)}}. \tag{28}$$

When there are similarities of velocities and pressure fields under different Reynolds numbers, the energy loss in the ejector nozzle is characterized by the Euler number alone [12]. This number depends on the geometric characteristic of the nozzle and can be represented as:

$$Eu = \frac{\Delta p}{\rho_c \nu_N^2}. \tag{29}$$

Here, Δp and ν_N are the pressure drop and the cutting fluid velocity in the nozzle.

The pressure loss coefficient, ζ_N, is selected as the estimator of the ejector nozzle design and can be expressed through the Euler number as:

$$\zeta_N = 2\,Eu. \tag{30}$$

Substituting equation (30) into equation (19), we get:

$$\mu = \frac{1}{\sqrt{(1 + 2\,Eu)}}. \tag{31}$$

Thus, the Euler number can be chosen as the initial characteristic of the nozzle, which defines the pressure loss and discharge coefficients.

The experiments were conducted in order to study:

(1) the influence of the nozzle's design on its hydraulic resistance and

(2) the suction capabilities of the different types of nozzles.

The eight different types of ejector nozzles are identified for study (Fig. 16, Table 1). For each type, the experimental relation $\zeta_N = f(Re)$ is obtained (Fig. 17). It can be seen from this figure that the minimum pressure loss corresponds to nozzle No. 5, with the conical cantor line under $\alpha = 22.5°$. However, this design is non-technological. Even small error of the axial position of the inner tube leads to a change in the nozzle size, that is a change of modulus m in the range of 15–7. Nozzle No. 2, with $\alpha = 12°$, is also characterized by a small pressure-loss coefficient, but it is difficult to make this nozzle using the thin inner tube. Based upon these considerations, a new design of ejector nozzle is proposed (Fig. 16, No. 7). This nozzle has a rounded, smooth entry, with conical and cylindrical parts. The Euler number for this nozzle ($Eu = 0.90$) is close to that for nozzle No. 5 ($Eu = 0.94$).

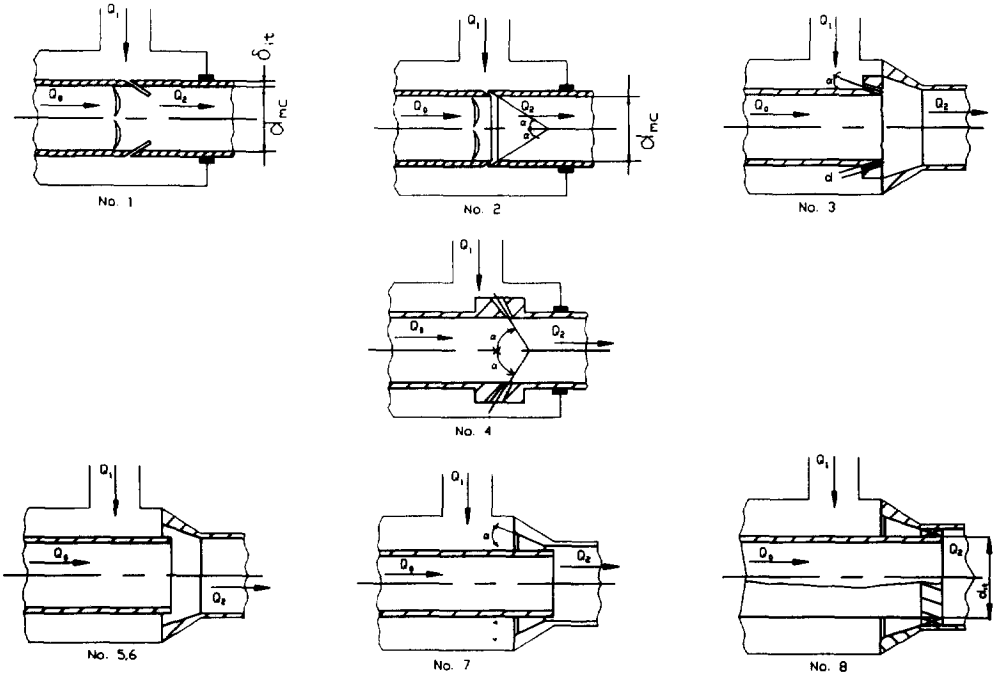

Fig. 16. Types of ejector nozzles used in the experiments: No. 1, Venturi; No. 2, Conical at the inner tube; No. 3, Multiple-Jet; No. 4, Vortex Multiple-Jet; Nos 5 and 6, Conical; No. 7, Combined; and No. 8, Vortex combined.

Table 1. Modulus of geometrical similarity, pressure-loss coefficient, and discharge coefficient of the ejector nozzles

No.	Type of nozzle	Geometrical characteristic	ζ_N	μ
1	Venturi	$m = \frac{\pi d_{mc}^2}{4nA_n}$ where n is the number of nozzles; A_n is the nozzle's cross-sectional area.	0.73	0.64
2	Conical at the inner tube	$m = \frac{(d_{mc}/2)^2}{\delta_0 B}$; $B = \delta_0 \cos^2\alpha + (d_{mc}/2)\cos\alpha$; $B = \delta_0 \cos^2\alpha + (d_{mc}/2)/\tan\alpha$ Here δ_0 is the nozzle width along the drill axis; α is the nozzle angle.	0.47	0.72
3	Multiple-jet	$m = \frac{d_{mc}^2}{nd_j^2}$	0.54	0.69
4	Vortex multiple-jet	Here d_j is the diameter of the jet holes	0.62	0.67
5	Conical $\alpha = 22.5°$	$m = \frac{\pi d_{mc}^2}{4A_N}$	0.07	0.94
6	Conical $\alpha = 45°$			
7	Combined	$m = \frac{d_{mc}^2}{d_{mc}^2 - d_{it}^2}$	0.12	0.90
8	Vortex combined		0.33	0.78

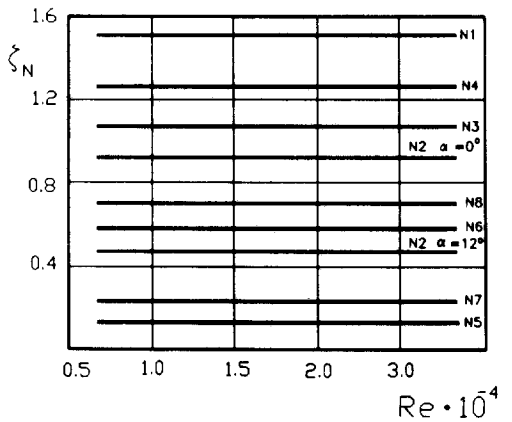

Fig. 17. Influence of the Reynolds numbers, Re, on the pressure loss coefficient ζ_N.

Efficiency of the ejector nozzle was evaluated according to its suction capability, which was defined by the value of the negative pressure (vacuum) depending upon the inlet head, H_1. The results of the study are shown in Fig. 18. Analysis of these results shows a correlation between the pressure-loss coefficient and suction capability of the ejector nozzle; that is, nozzles which are characterized by similar pressure-loss coefficients have approximately the same suction capability. Nozzle Nos 5 and 7 have the largest suction capabilities. As demonstrated in Fig. 18, the suction capability increases with an increase in the inlet head. The restriction factor for suction capability is cavitation in the mixing chamber, which occurs when the value of the vacuum exceeds 0.078 MPa. As indicated in the experiments, this value does not depend on the design parameters of the ejector nozzle or the ejector. The value of vacuum created by the ejector nozzle for a given operating head can be found in Fig. 18, and this value is one of the most important energy

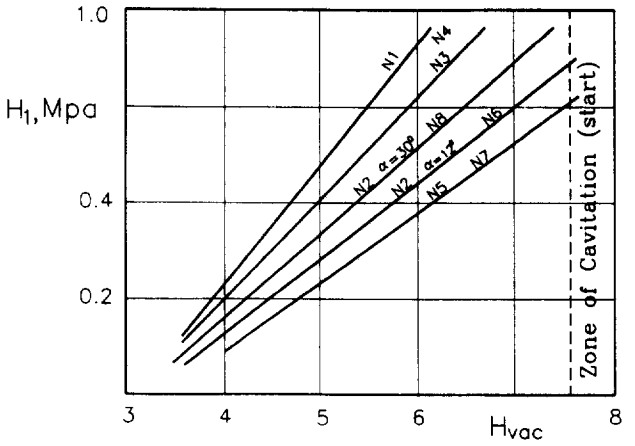

Fig. 18. Influence of the operating head, H_1, on the vacuum in the mixing chamber, H_{vac}.

characteristics of the ejector. The most common error is that this value is not considered when defining the position of the ejector nozzle in relation to the machining zone. The correct positioning of the ejector nozzle can be verified by the following inequality:

$$H_{vac} \geq \Delta h_s . \tag{32}$$

Here, Δh_s is the head loss of the cutting fluid–chip mixture, swarf (including the elevation of the nozzle position, relative to the machining zone), along the distance between the machining zone and the ejector nozzle.

Losses due to change of location, past the mixing chamber, can be reduced by installing a diffuser between the mixing chamber and the other part of the chip removal channel (Fig. 12). The coefficient of the hydraulic loss in diffusion is determined by the non-dimensional characteristics $h = f(q, \alpha_d)$. Under a small diffuser angle, α_d (up to 8°) and ratio l_d/d_{mc} = 2–4, the hydraulic resistance coefficient in the diffuser is ζ_d = 0.5–0.7 (lower values correspond to the smaller ratios l_d/d_{mc}) for a wide range of ejector parameters.

In order to define the energy loss in the mixing chamber, the equation for energy balance was used. The nozzle Nos 1, 7 and 8 were selected for this investigation and the following results for the pressure-loss coefficients were obtained:

$$\zeta_{mc1} = 1.497 \times m^{1.407} \times q^{0.157 \cdot \log m - 0.661} \tag{33}$$

$$\zeta_{mc7} = 0.0241 \times m^{2.451} \times q^{-1.661} \tag{34}$$

$$\zeta_{mc8} = 0.0138 \times m^{2.331} \times q^{0.079 \cdot \log m + 1.468} . \tag{35}$$

The relationship $\zeta_{mc} = f(q,m)$ for nozzle No. 7 is shown in Fig. 19. It can be seen that an increase in the modulus m leads to increased energy loss in the mixing chamber. Due to an increase in the value of m, the velocities of re-circulation and operating flows increase, resulting in energy loss.

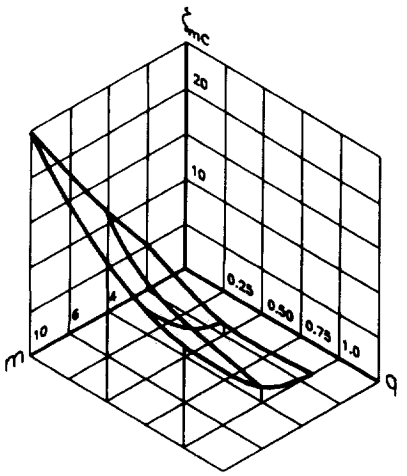

Fig. 19. Effect of modulus m and relative flow rate, q, on the pressure loss coefficient ζ_{mc} for nozzle No. 7.

Therefore, the experimental comparison of the different types of ejector nozzles shows that the combined ejector nozzle (nozzle No. 7) is the most efficient among the samples used.

APPENDIX B: CALCULATION OF THE EJECTOR POSITION IN THE HYDRAULIC SYSTEM OF THE EJECTOR DRILL

Calculation of the ejector position can be carried out as follows.

(1) Calculate the critical cutting fluid velocity, V_{cr}, as the velocity corresponding to the beginning of reliable chip transportation.

(2) Calculate the re-circulation flow rate as:

$$Q_0 = V_{cr} \cdot A_{in}. \tag{36}$$

(3) Calculate the cross-sectional area of the ejector nozzle, using the selected modulus m = 3.5–4.0, then calculate S_{BD} [equation (22)].

(4) Choose the relative flow rate, corresponding to the maximum efficiency as q = 0.4–0.6 (Fig. 10).

(5) Calculate the operating flow rate, Q_1 as:

$$Q_1 = Q_0 \cdot q. \tag{37}$$

(6) Calculate the required operating head [equation (18) when $Q = Q_1$].

(7) Calculate the inlet flow rate as:

$$Q_\Sigma = Q_0 + Q_1. \tag{38}$$

(8) Calculate the hydraulic-resistance coefficient S_{BC} from equation (23).

(9) Calculate the ejector position (length l_o) from equation (21).

(10) Verify, using equation (32).

(11) Calculate the relative head, h, by using equation (11) for the independent ejector design or equation (15) for the dependent ejector design. This calculated value of h can then be compared to the maximum value of h under given conditions (Fig. 11). The difference between the two values shows how far the chosen regime is from the optimal.

(12) Calculate the head, H_2 [equation (1)].

(13) Verify the condition:

$$H_2 >= \Sigma h \tag{39}$$

where Σh is the total hydraulic head loss.

If inequality (39) holds, the calculations are complete. Otherwise, one must reduce the relative flow rate in accordance with Fig. 11 in order to achieve the required value of h and therefore H_2.